

## Supplementary information

### **All-inorganic Quantum Dot Assisted Enhanced Charge Extraction Across the Interfaces of Bulk Organo-Halide Perovskite for Efficient and Stable Pin-hole Free Perovskite Solar Cells**

Dibyendu Ghosh,<sup>1#</sup> Dharendra K. Chaudhary,<sup>1#</sup> Md. Yusuf Ali,<sup>1</sup> Kamlesh Kumar Chauhan,<sup>2</sup> Sayan Prodhan,<sup>3</sup> Sayantan Bhattacharya,<sup>3</sup> Barun Ghosh,<sup>4</sup> P. K. Datta,<sup>3</sup> Sekhar C. Ray,<sup>4</sup> and Sayan Bhattacharyya<sup>1\*</sup>

<sup>1</sup>*Department of Chemical Sciences, and Centre for Advanced Functional Materials, Indian Institute of Science Education and Research (IISER) Kolkata, Mohanpur 741246, India*

<sup>2</sup>*Department of Electrical Engineering, Indian Institute of Technology (IIT) Kharagpur, Kharagpur – 721302, India*

<sup>3</sup>*Department of Physics, Indian Institute of Technology (IIT) Kharagpur, Kharagpur – 721302, India*

<sup>4</sup>*Department of Physics, CSET, University of South Africa, Private Bag X6, Florida, 1710, Science Campus, Christiaan de Wet and Pioneer Avenue, Florida Park, Johannesburg, South Africa*

\* Email for correspondence: sayanb@iiserkol.ac.in

# Equal contribution

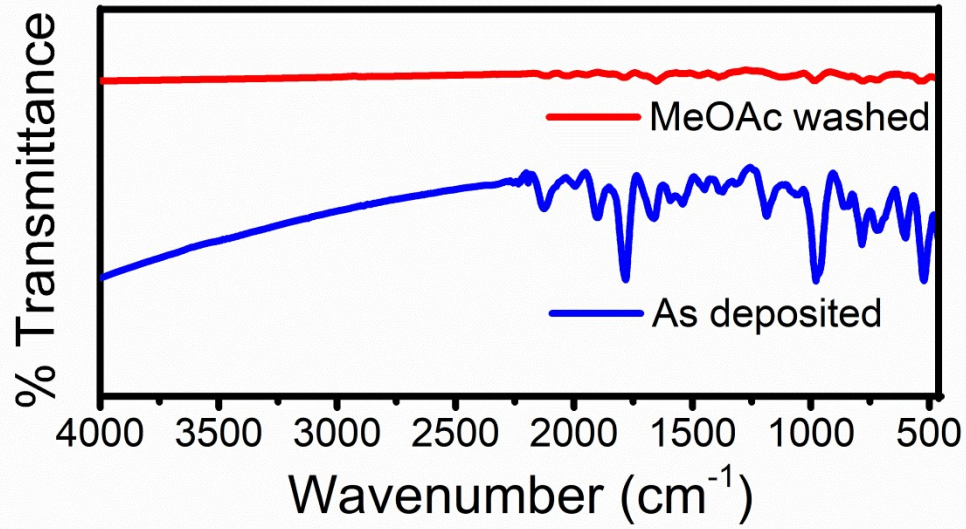


**Fig. S1.** FTIR spectra of a representative CsPbBr<sub>3</sub> QD modified bulk perovskite film, unwashed (blue line) and washed with methyl acetate solution of lead nitrate (red line).

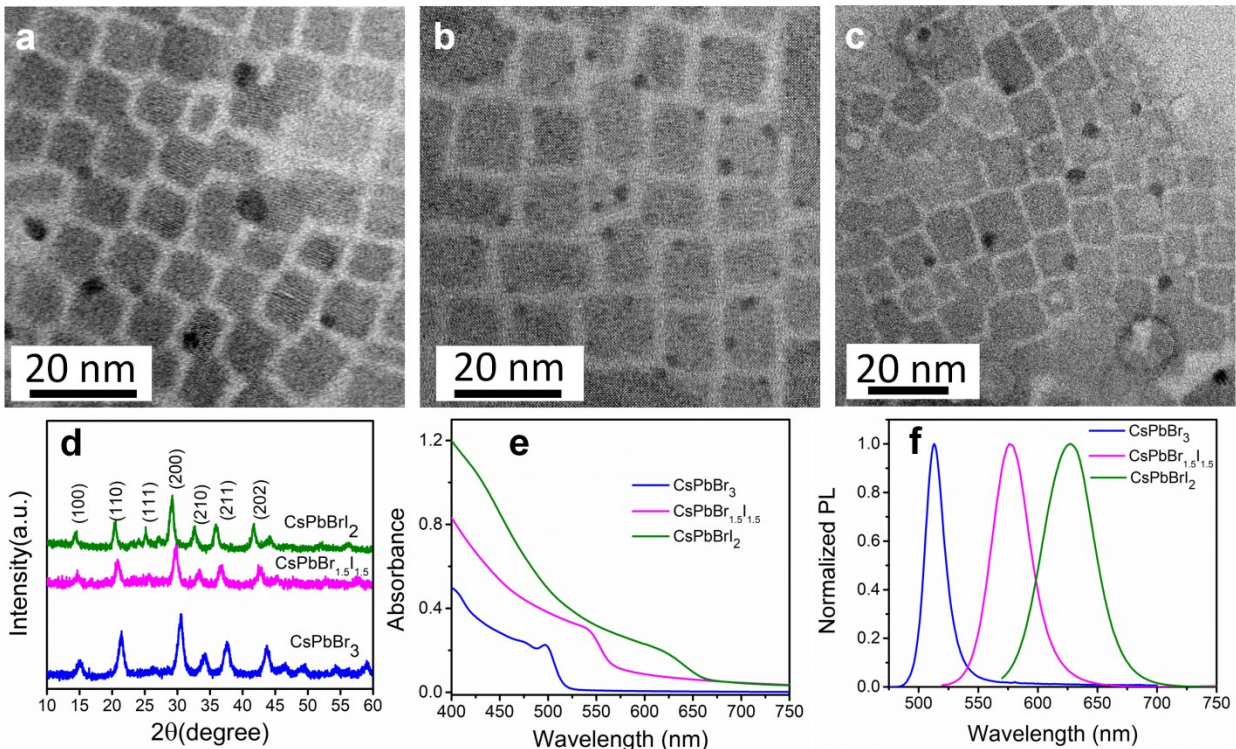


**Fig. S2.** TEM images of (a) CsPbBr<sub>3</sub>, (b) CsPbBr<sub>1.5</sub>I<sub>1.5</sub> and (c) CsPbBrI<sub>2</sub> QDs. (d) XRD patterns, (e) UV-vis and (f) PL spectra of the QDs.

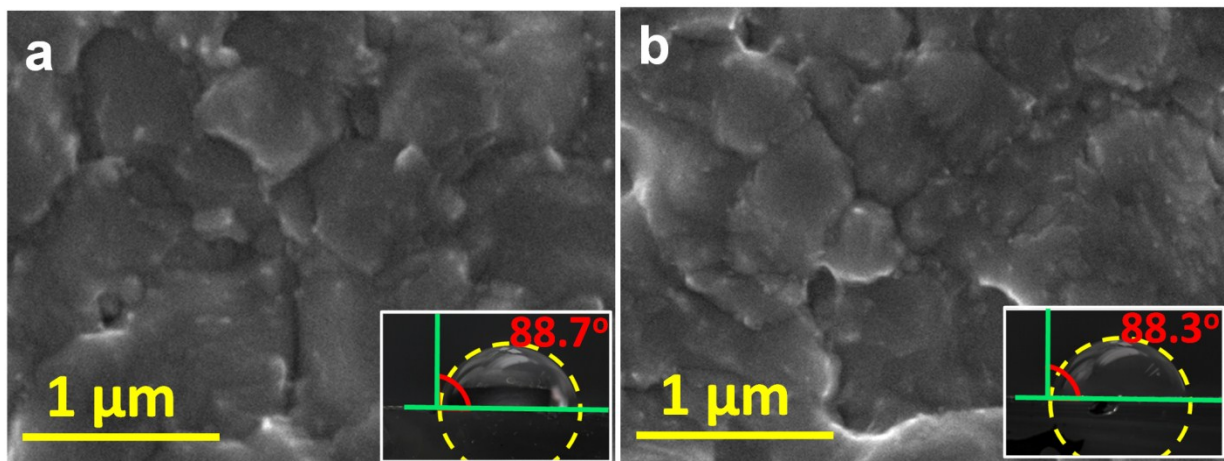


**Fig. S3.** FE-SEM images of (a) CsPbBr<sub>3</sub> and (b) CsPbBr<sub>2</sub> modified perovskite films. Insets show the respective contact angles.

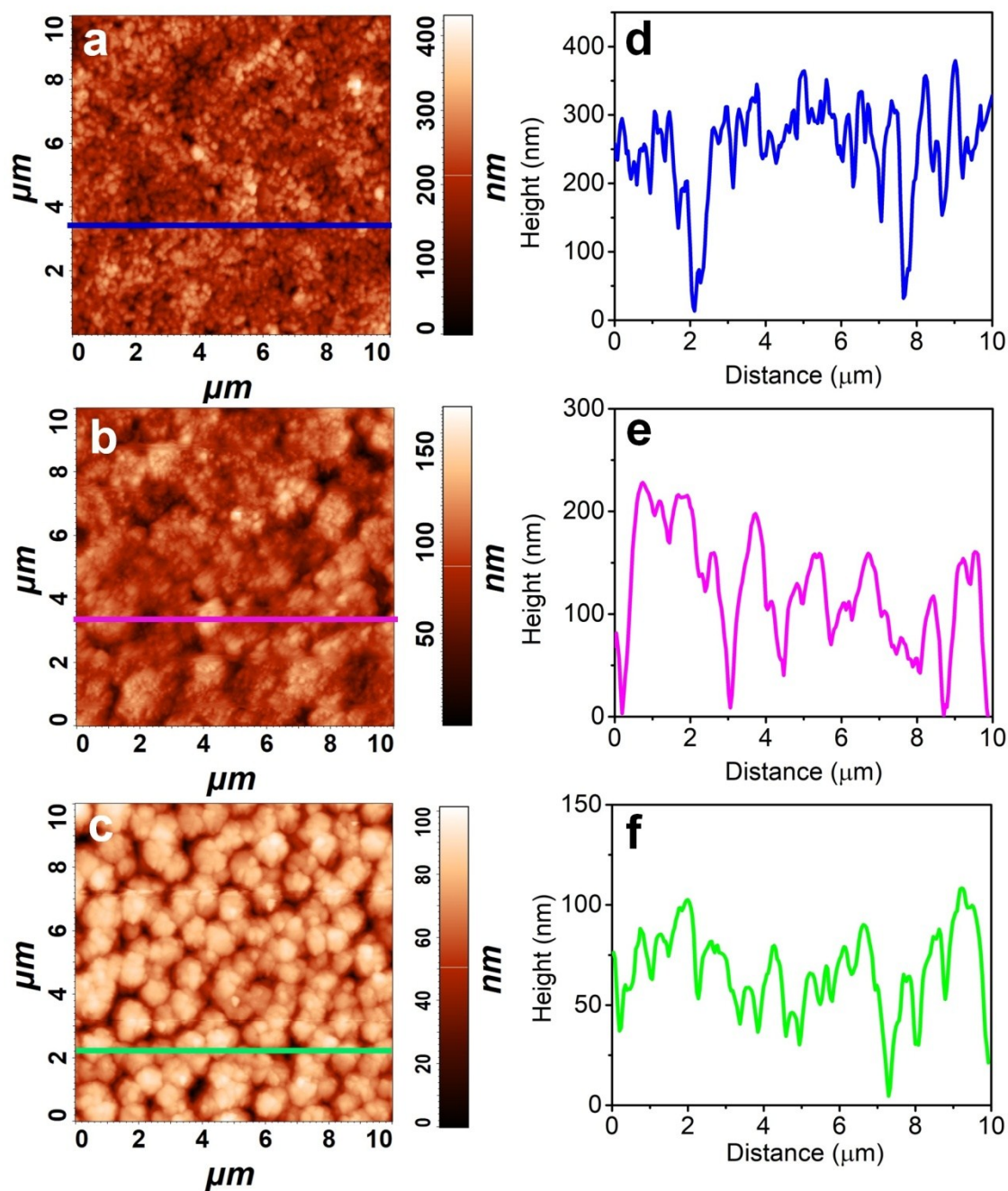


**Fig. S4.** (a-c) AFM images of the unmodified, CB modified and CsPbBr<sub>1.5</sub>I<sub>1.5</sub> QD modified perovskite (CH<sub>3</sub>NH<sub>3</sub>PbI<sub>3-x</sub>Cl<sub>x</sub>) thin films deposited on FTO/c-TiO<sub>2</sub>/m-TiO<sub>2</sub>, respectively, employed later for solar cell fabrication. (d-f) Height profiles from AFM surface analysis of the corresponding perovskite films.

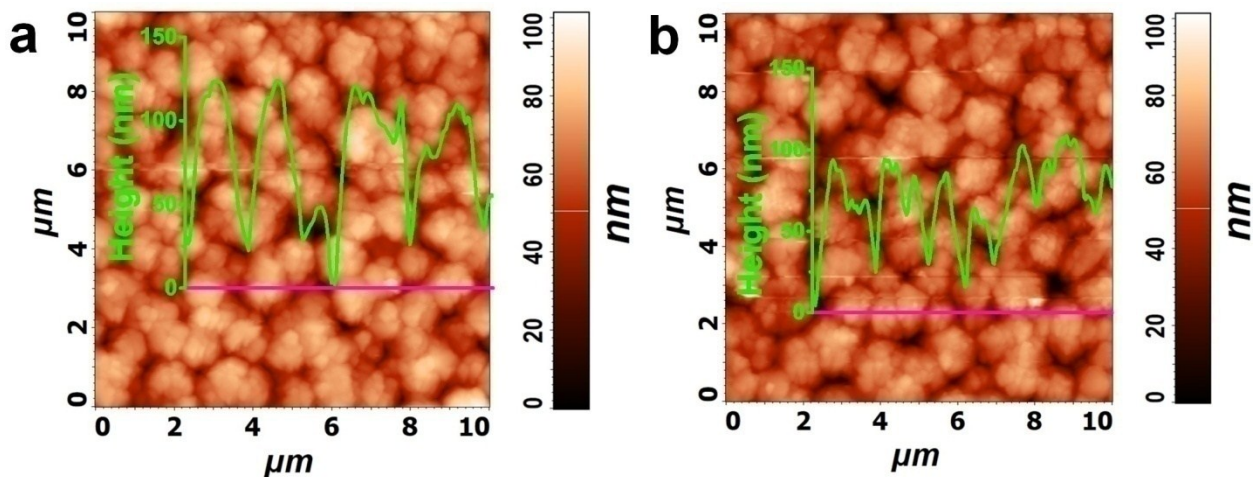


**Fig. S5.** AFM images of (a) CsPbBr<sub>3</sub> and (c) CsPbBrI<sub>2</sub> QD modified perovskite films. Insets show the respective height profile.

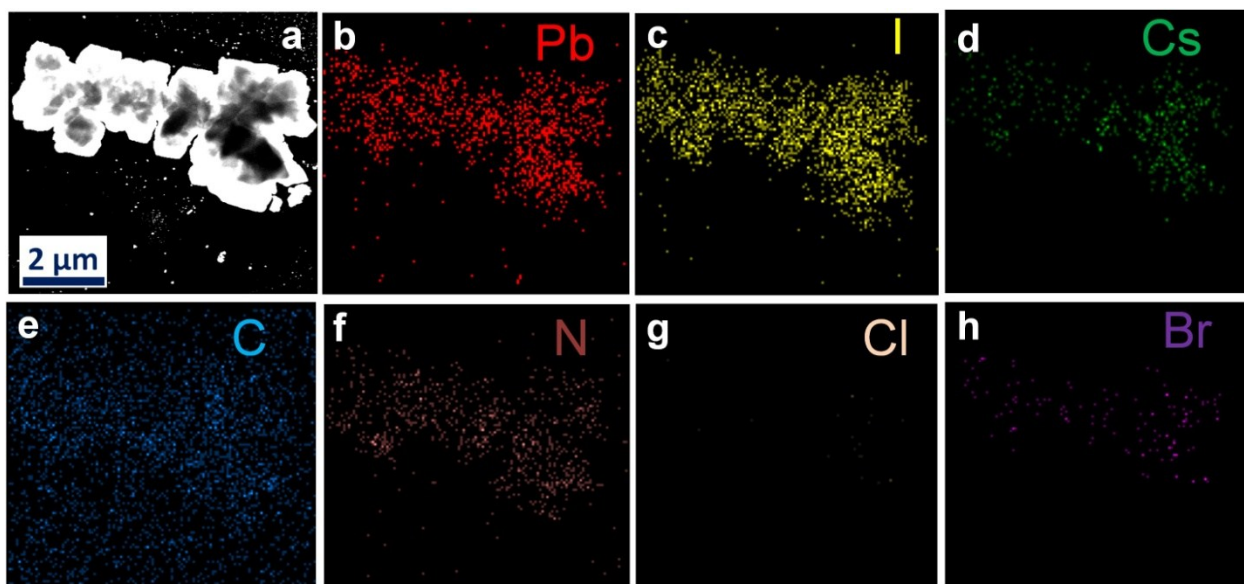


**Fig. S6.** (a) HAADF-STEM image of CsPbBr<sub>1.5</sub>I<sub>1.5</sub> QD modified CH<sub>3</sub>NH<sub>3</sub>PbI<sub>3-x</sub>Cl<sub>x</sub> perovskite grains taken by scratching the films from FTO substrate. (b-h) Elemental maps of the representative elements. No trace of chlorine (Cl) was observed since Cl escapes in the form of CH<sub>3</sub>NH<sub>3</sub>Cl during annealing of the perovskite films, consistent with earlier reports.<sup>S1,S2</sup>

**Table S1.** Parameters from UV-vis absorption and PL spectra.

| <b>Samples</b>                                     | <b>Crystallite size (nm)</b> | <b>Absorption onset (nm)</b> | <b>Band Gap (eV)</b> | <b>PL peak position (nm)</b> | <b>Stokes shift (nm)</b> |
|--|------------------------------|------------------------------|----------------------|------------------------------|--------------------------|
| Unmodified   | 31                           | 775                          | 1.60                 | 769                          | 6                        |
| CB modified  | 68                           | 778                          | 1.59                 | 769                          | 9                        |
| CsPbBr <sub>3</sub> QD modified                    | 71                           | 761                          | 1.63                 | 764                          | 3                        |
| CsPbBr <sub>1.5</sub> I <sub>1.5</sub> QD modified | 73                           | 766                          | 1.62                 | 762                          | 4                        |
| CsPbBrI <sub>2</sub> QD modified                   | 72                           | 764                          | 1.62                 | 756                          | 8                        |

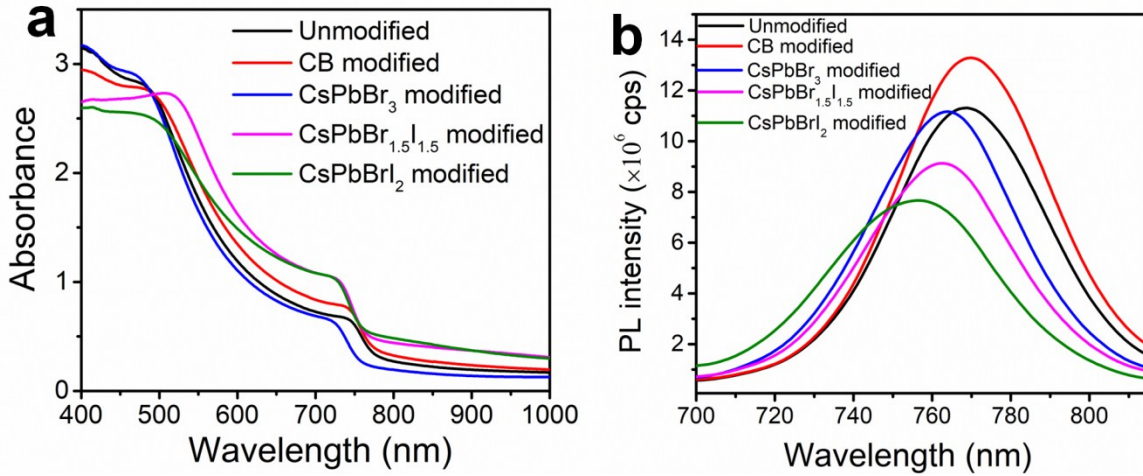


**Fig. S7.** (a) UV-vis and (b) PL spectra of unmodified, CB modified and QD modified perovskite films deposited on *c*-TiO<sub>2</sub> coated glass substrate. The different QDs used are CsPBr<sub>3</sub>, CsPbBr<sub>1.5</sub>I<sub>1.5</sub> and CsPbBrI<sub>2</sub>.

The absorption spectrum of CH<sub>3</sub>NH<sub>3</sub>PbI<sub>3-x</sub>Cl<sub>x</sub> shows good coverage of solar spectrum and the band gap estimated from absorption onset is ~1.60 eV. Enhancement in absorption of CB, CsPbBr<sub>1.5</sub>I<sub>1.5</sub> and CsPbBrI<sub>2</sub> modified films are observed which is due to formation of larger grains. Larger grain size increases the distance of light propagation within the perovskite due to backscattering of incident light that ultimately enhances the absorbance in comparison to unmodified films.<sup>S3</sup> Band gap increases slightly after CB, CsPbBr<sub>1.5</sub>I<sub>1.5</sub> and CsPbBrI<sub>2</sub> QD modifications because of bond formation between bulk perovskite (PbI<sub>6</sub><sup>-</sup> framework) and more electronegative Br<sup>-</sup> ions in the QDs.

The unmodified film shows the PL emission peak near absorption band edge position whereas after CB modification, a small blue shift and increase in emission peak intensity is observed. The formation of larger grains by CB modification reduces the grain boundaries consisting of amorphous intergranular interfaces which thereby decrease the recombination centers. After QD modification, PL intensity is quenched and a significant blue shift is observed. The quenching in PL emission occurs due to hole transfer from perovskite to QDs and transfer of electrons to *c*-TiO<sub>2</sub>. The blue shift can be attributed to the reduction of recombination centers due to formation of larger gains as well as small increase in band gap.

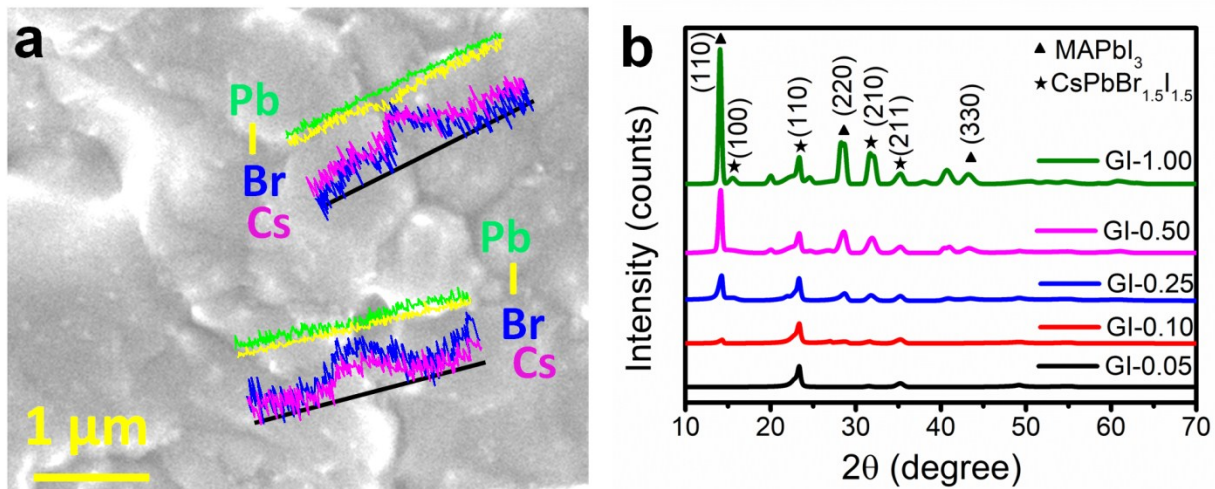


**Fig. S8.** (a) Elemental line scan at the grain boundaries and (b) GI-XRD patterns at different grazing angles for CsPbBr<sub>1.5</sub>I<sub>1.5</sub> QD modified perovskite films.

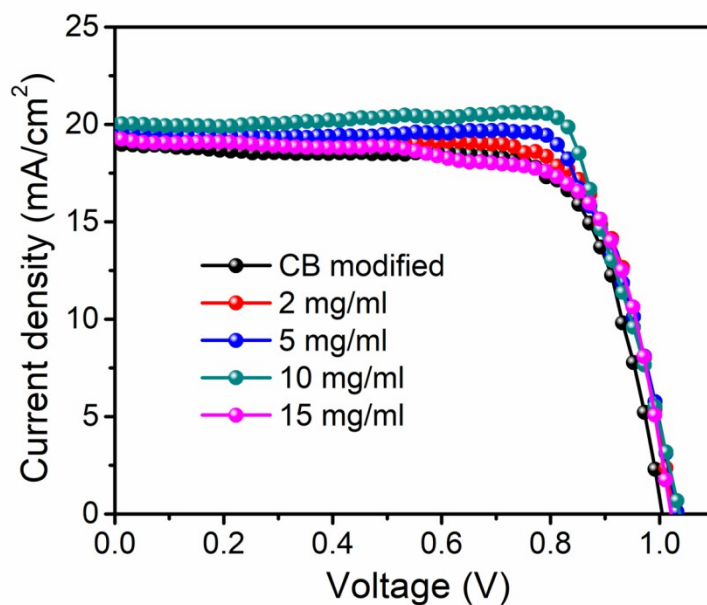


**Fig. S9.** J-V characteristics of the devices under illumination with different concentrations of CsPb CsPbBr<sub>1.5</sub>I<sub>1.5</sub> QDs, from 2 to 15 mg/ml in CB.

PCE increases from 14.72 to 16.51% for an optimum concentration of 10 mg/ml and decreases beyond that. After increasing the QD concentration beyond 10 mg/ml the over

concentrated QDs form a separate thin layer over the bulk perovskite and thereby the charge transportation is hindered.

**Table S2:** Photovoltaic parameters with different concentrations of CsPbBr<sub>1.5</sub>I<sub>1.5</sub> QDs.

| Concentration of QDs (mg/ml) | V <sub>oc</sub> (V) | J <sub>sc</sub> (mA/cm <sup>2</sup> ) | Fill Factor | Efficiency (%) |
|------------------------------|---------------------|---------------------------------------|-------------|----------------|
| 2                            | 1.02                | 19.76                                 | 0.73        | 14.72 ± 0.25   |
| 5                            | 1.03                | 19.70                                 | 0.75        | 15.39 ± 0.32   |
| 10                           | 1.03                | 20.05                                 | 0.79        | 16.51 ± 0.20   |
| 15                           | 1.03                | 19.23                                 | 0.71        | 14.06 ± 0.38   |

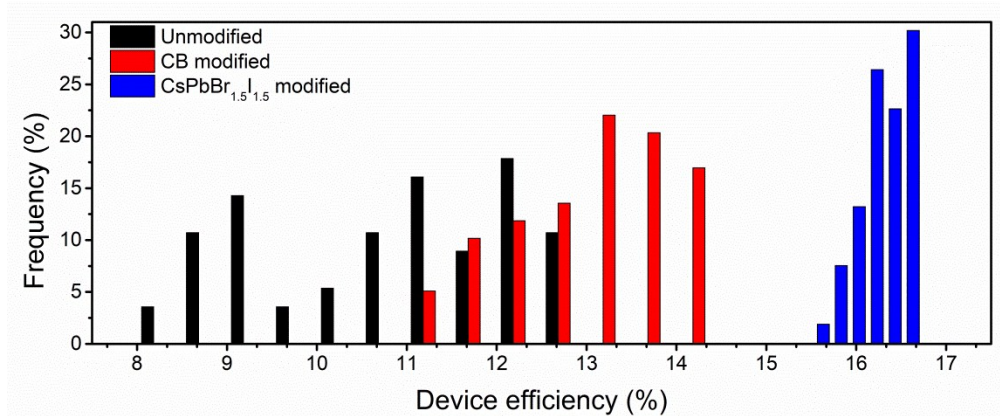


**Fig. S10.** Distribution of efficiency over 100 devices with unmodified, CB modified and CsPbBr<sub>1.5</sub>I<sub>1.5</sub> QD modified bulk perovskite absorbers.

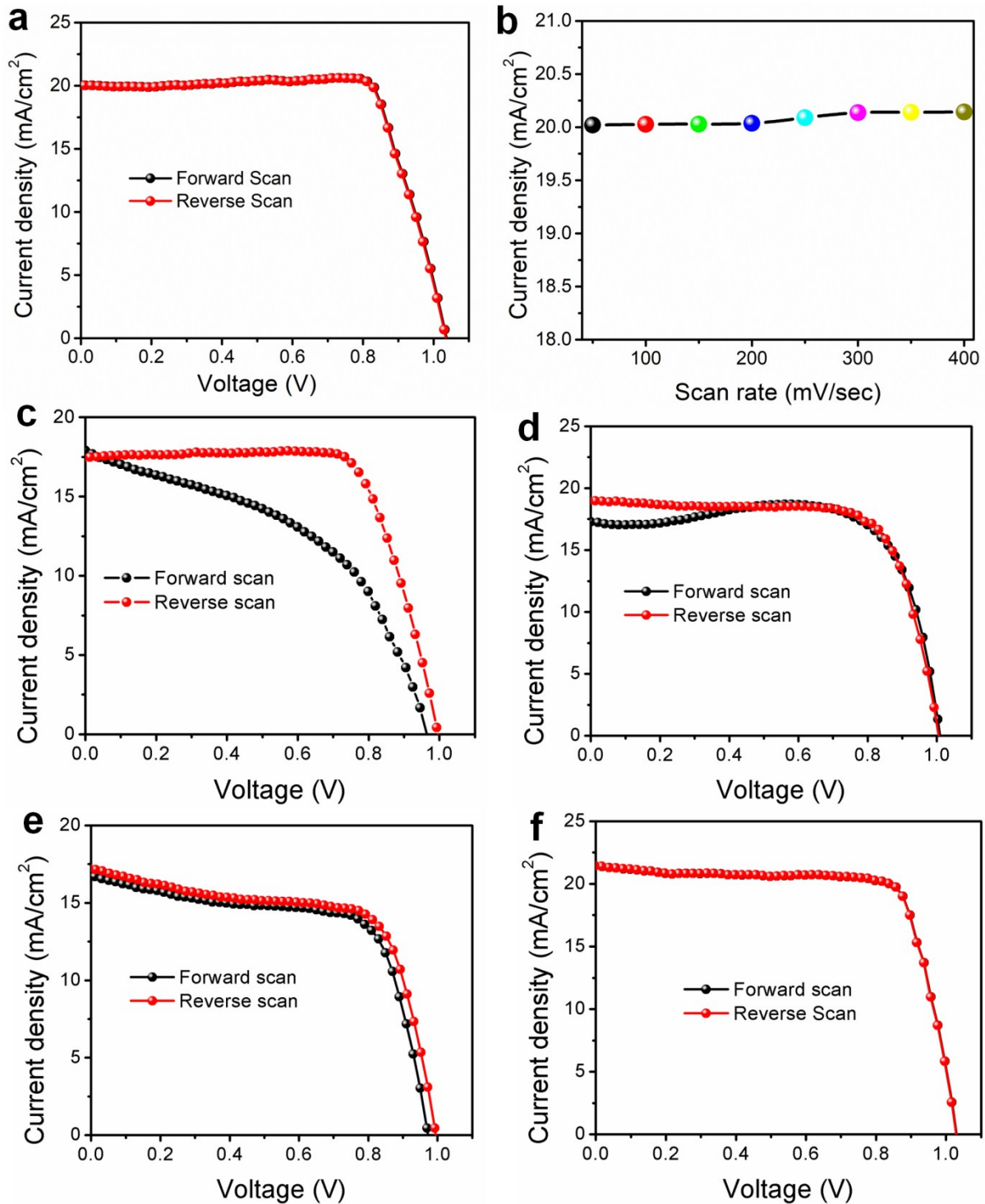


**Fig. S11.** (a) J-V characteristics of CsPbBr<sub>1.5</sub>I<sub>1.5</sub> QDs modified devices in forward and reverse scan direction and (b) J<sub>SC</sub> values of same devices at different scan rate. J-V characteristics of devices under forward and reverse scan direction for (c) unmodified, (d) CB modified, (e) CsPbBr<sub>3</sub> modified, and (f) CsPbBrI<sub>2</sub> modified.

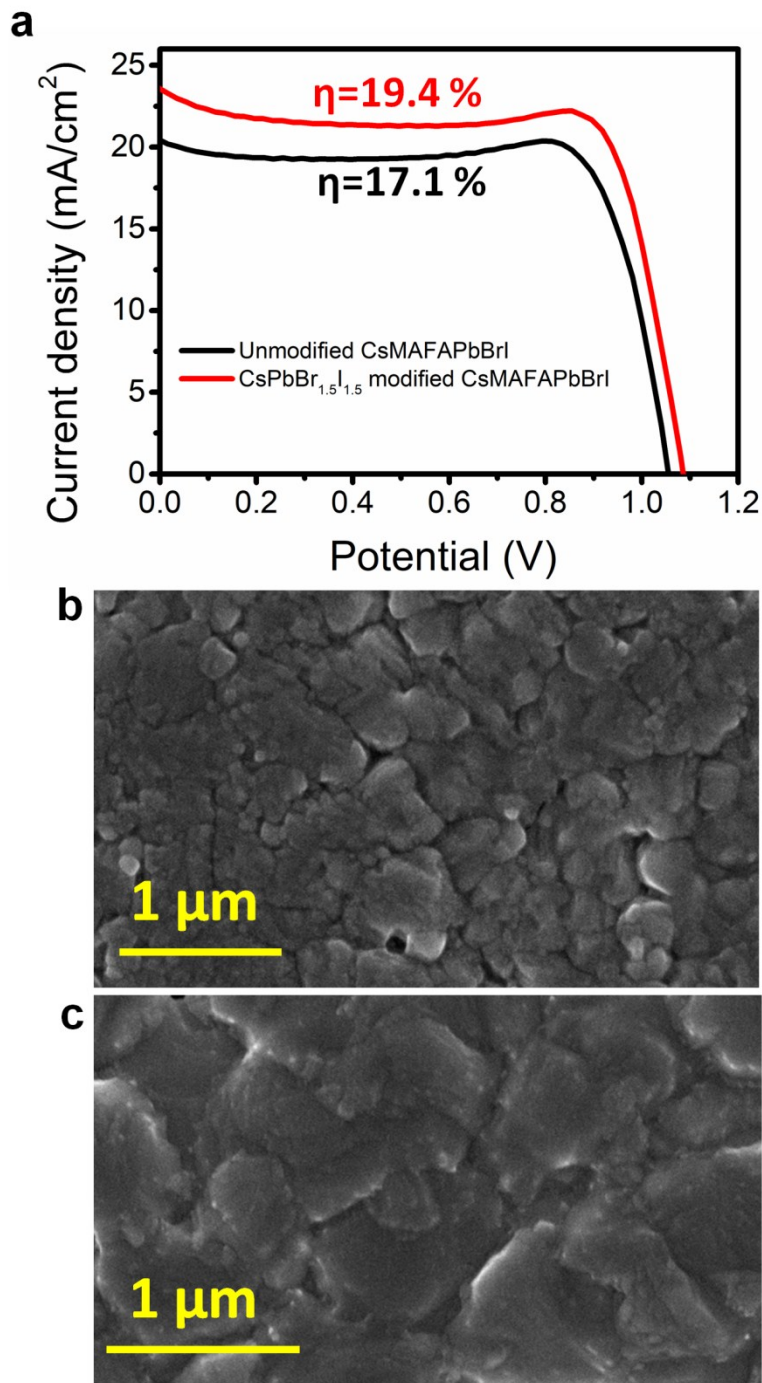


**Fig. S12.** (a) J-V curves for unmodified (black line) and representative CsPbBr<sub>1.5</sub>I<sub>1.5</sub> QD modified (red line) bulk Cs<sub>0.05</sub>(MA<sub>0.17</sub>FA<sub>0.83</sub>)<sub>0.95</sub>Pb(I<sub>0.83</sub>Br<sub>0.17</sub>)<sub>3</sub> (represented as CsMAFAPbBrI) device under 1 sun illumination. In the unmodified CsMAFAPbBrI device,  $J_{\text{SC}}$ ,  $V_{\text{OC}}$  and FF are 20.45  $\text{mA}/\text{cm}^2$ , 1.06 V and 0.78, respectively. After QD modification,  $J_{\text{SC}}$ ,  $V_{\text{OC}}$  and FF become 23.47  $\text{mA}/\text{cm}^2$ , 1.08 V and 0.77, respectively. FESEM images of the (b) unmodified and (c) CsPbBr<sub>1.5</sub>I<sub>1.5</sub> QD modified CsMAFAPbBrI films.

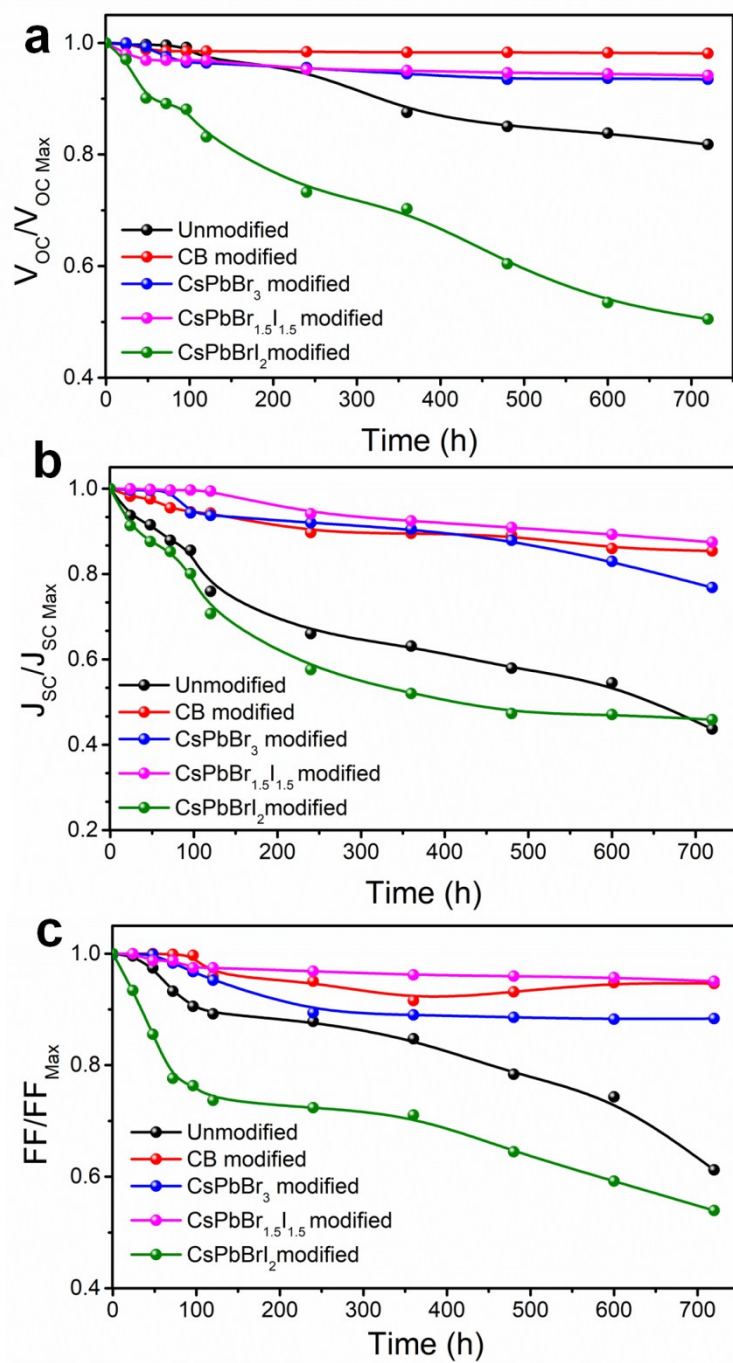


**Fig. S13.** Degradation profile of solar cell performance in terms of normalized device parameters (a)  $V_{OC}$ , (b)  $J_{SC}$  and (c)  $FF$  according to ISOS-D1 protocols.

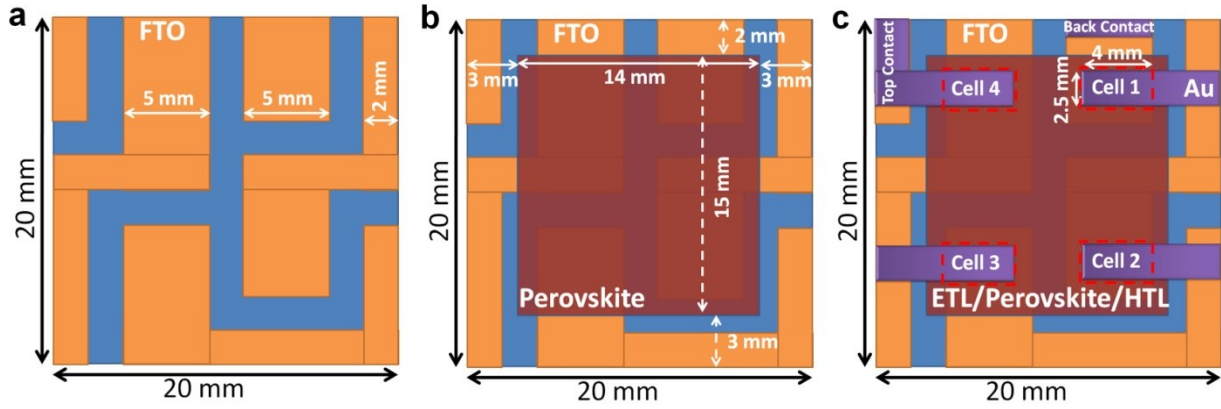


**Fig. S14.** FTO patterning and mask design for integration of four cells in series. (a) FTO patterning, (b) ETL, perovskite and HTL layer deposition, and (c) top metal contact.

**Table S3:** Nyquist fitting parameters for the unmodified and modified PV devices measured at zero bias and 1 sun illumination.

| Samples   | $R_S$<br>( $\Omega$ ) | $R_{CT}$<br>( $\Omega$ ) | $C_g$<br>(nF) | $C_S$<br>( $\mu$ F) | $\tau_e$<br>(ms) |
|---|-----------------------|--------------------------|---------------|---------------------|------------------|
| Unmodified                                      | 90.66                 | 1695                     | 38.41         | 0.94                | 0.81             |
| CB modified                                     | 109.6                 | 1133                     | 33.26         | 0.61                | 1.01             |
| CsPbBr <sub>3</sub> modified                    | 194.4                 | 894.4                    | 53.36         | 0.31                | 2.62             |
| CsPbBr <sub>1.5</sub> I <sub>1.5</sub> modified | 111                   | 555.7                    | 48.91         | 0.45                | 4.54             |
| CsPbBrI <sub>2</sub> modified                   | 118.8                 | 591                      | 61.74         | 0.47                | 4.06             |

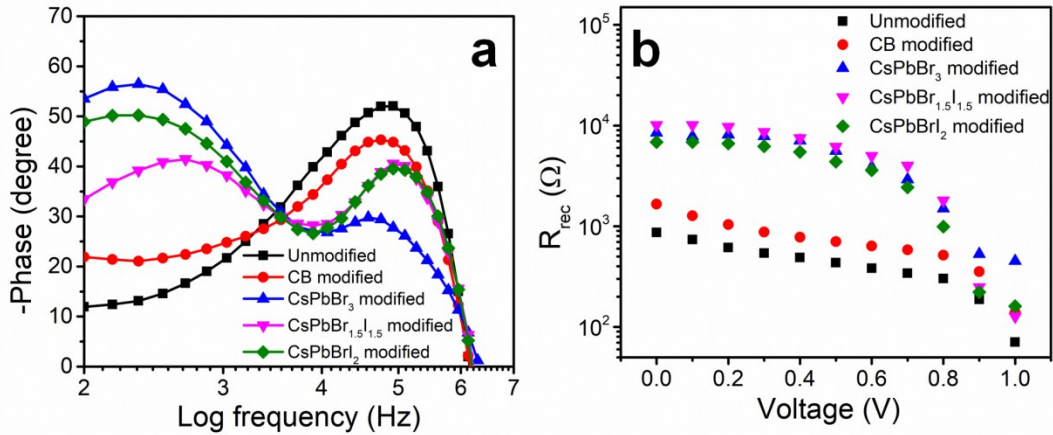


**Fig. S15.** (a) Bode plots measured at zero bias and (b)  $R_{\text{rec}}$  measured at different applied bias for the unmodified and CB, CsPbBr<sub>3</sub>, CsPbBr<sub>1.5</sub>I<sub>1.5</sub> and CsPbBrI<sub>2</sub> QD modified samples measured in the frequency range from 2 MHz to 100 Hz under simulated 100 mW cm<sup>-2</sup> AM1.5G illumination.

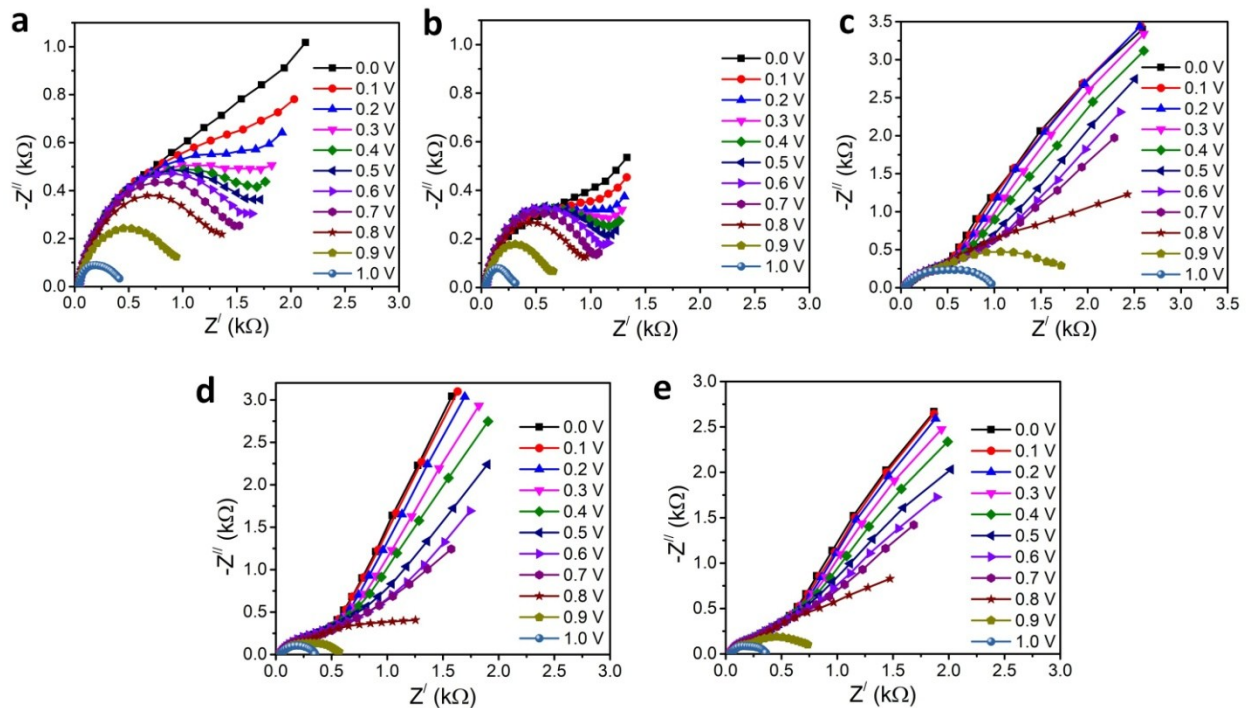


**Fig. S16.** Nyquist plots at different applied bias for (a) unmodified, (b) CB modified, (c) CsPbBr<sub>3</sub> QD modified, (d) CsPbBr<sub>1.5</sub>I<sub>1.5</sub> QD modified and (e) CsPbBrI<sub>2</sub> QD modified devices measured at different applied bias and frequency ranging from 2 MHz to 100 Hz under simulated 100 mW cm<sup>-2</sup> AM1.5G illumination.

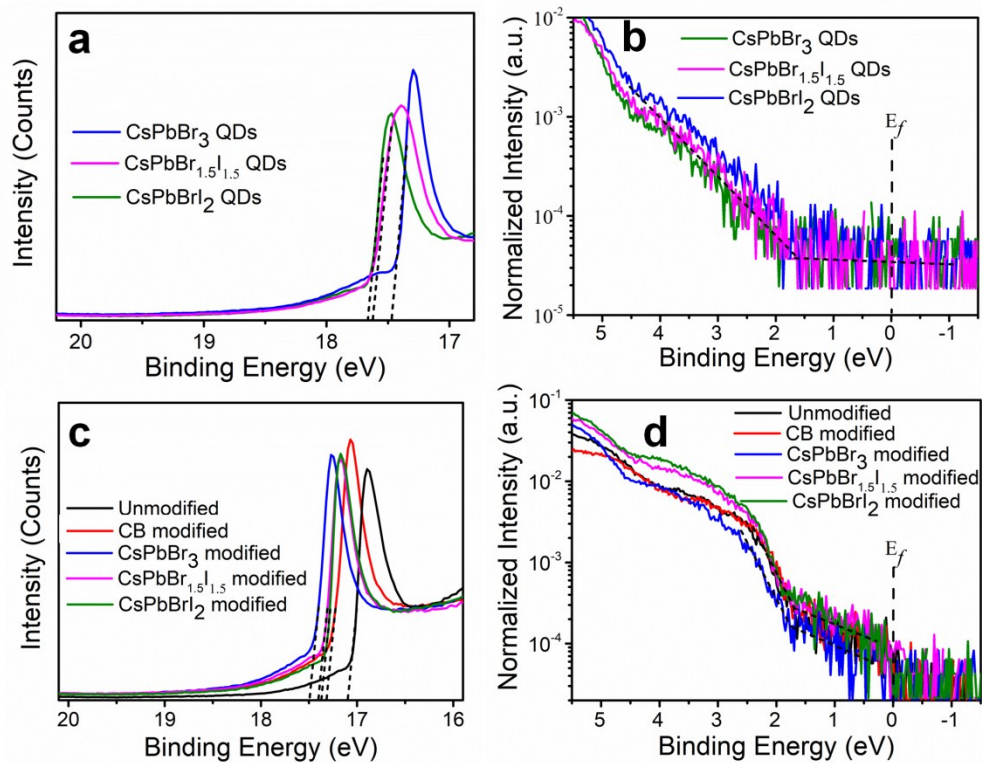


**Fig. S17.** UPS spectra of CsPbBr<sub>3</sub>, CsPbBr<sub>1.5</sub>I<sub>1.5</sub> and CsPbBrI<sub>2</sub> QDs: (a) cut-off region for measuring work function and (b) valance band spectra. UPS spectra of unmodified, CB modified and QD modified bulk perovskite: (c) cut-off region and (d) valance band spectra.

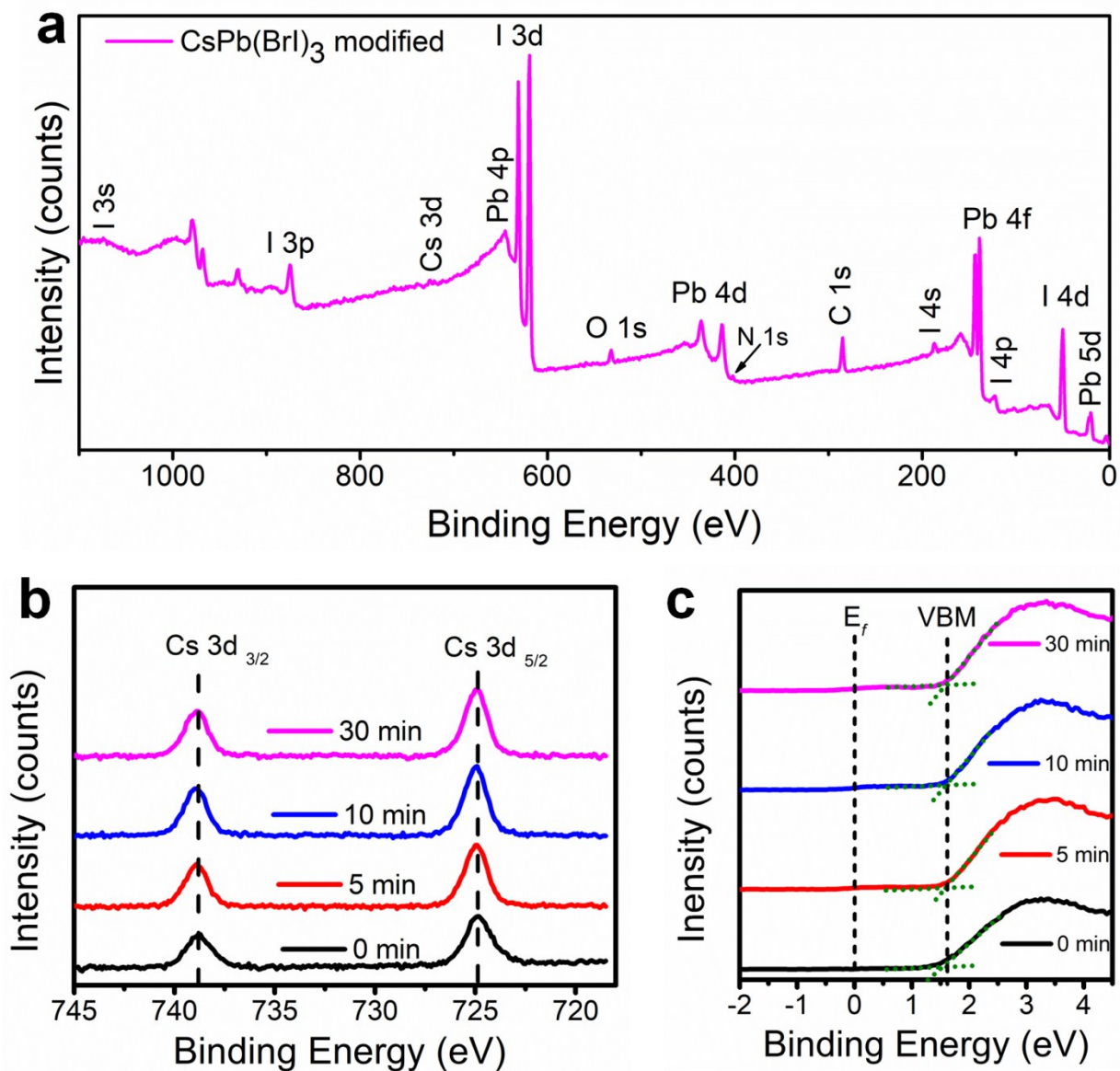


**Fig. S18.** (a) XPS survey scan of CsPbBr<sub>1.5</sub>I<sub>1.5</sub> QD modified bulk CH<sub>3</sub>NH<sub>3</sub>PbI<sub>3-x</sub>Cl<sub>x</sub> perovskite. (b) Cs 3d spectra and (c) valance band spectra for CsPbBr<sub>1.5</sub>I<sub>1.5</sub> QD modified bulk perovskite at different time of surface etching *via* Ar sputtering.

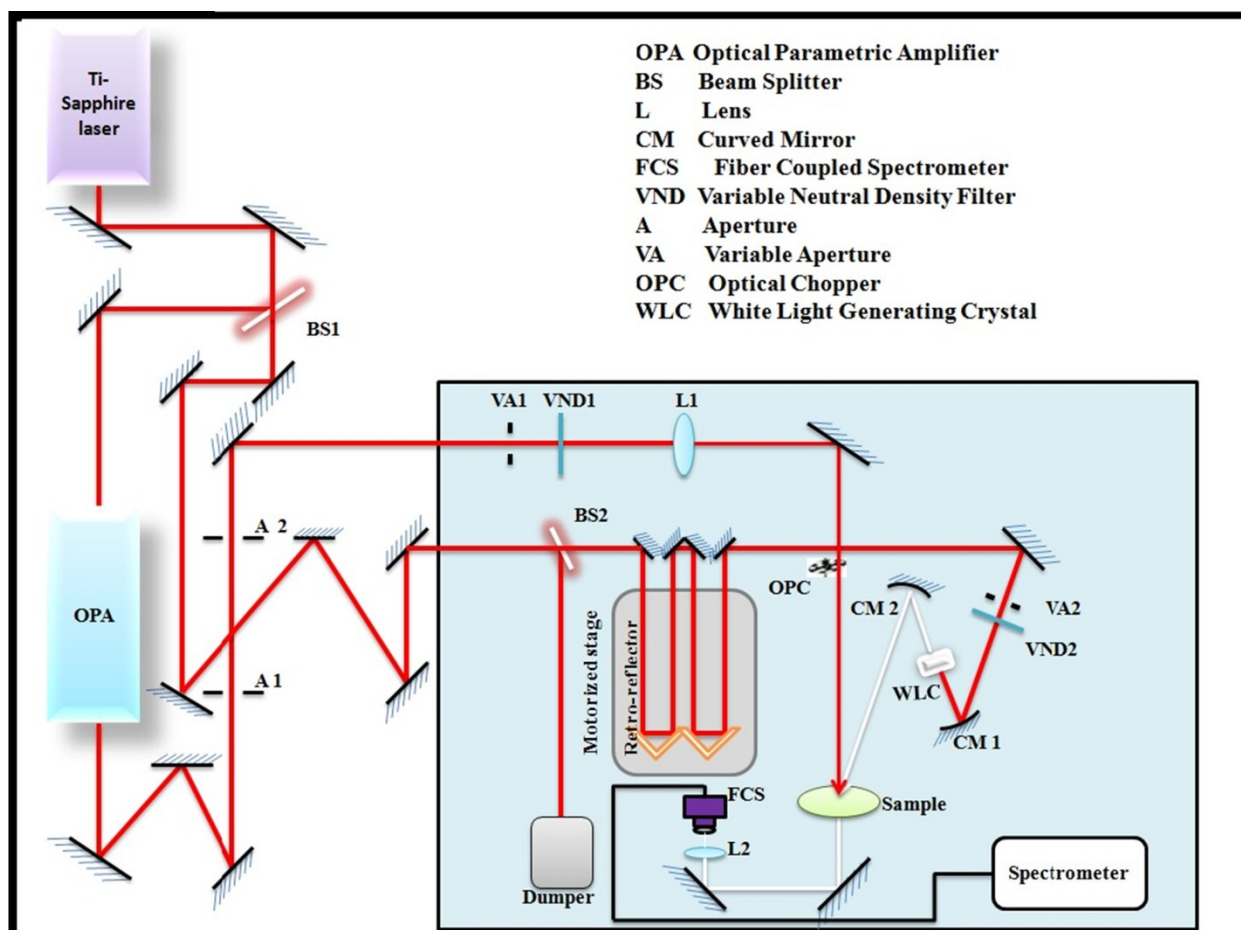


**Fig. S19.** Schematic of ultrafast transient absorption spectroscopy setup.

### Transient Absorption Spectroscopy

Ultrafast transient absorption spectroscopy (TAS) is a powerful tool for determining the charge carrier transfer, charge carrier dynamics, recombination dynamics and carrier relaxation process.<sup>S1-S6</sup> The change in absorbance induced by the pump pulse is measured in terms of

logarithmic ratio of intensity with and without pump excitation  $\left( \Delta A = \log \frac{I_{noex}}{I_{ex}} \right)$ . The present

TAS measurements are performed under ambient atmospheric conditions, but the effects of humidity degradation and oxygen infection of the perovskite film are not considered in the present work. The fs-TA measurement takes 20 min duration to complete the pump probe measurement on each sample. Figure S15 shows the TAS experimental setup utilizing a regenerative amplified Ti: sapphire laser system from Coherent (808 nm, 80 fs, 3 mJ/pulse, and 1 kHz repetition rate). The 30/70 beam splitter splits the 808 nm laser beam into two parts; the

reflected part is used as pump beam for TOPAS optical parametric amplifier. It generates the pump beam for the TAS experiment within 250-1500 nm band. For the present work, the pump beam is of 480 nm, attenuated by variable neutral density filter set at the fluence of  $7.5 \mu\text{J}/\text{cm}^2$  focused on the sample. The transmitted part of 808 nm laser pulse again splits into two beams, the one with less than 10% power was first transmitted through retro reflector stage to generate the time delay between pump and probe followed by a neutral density filter and focused into  $\text{CaF}_2$  crystal to generate a white light continuum (WLC) from 350 nm to 950 nm used as probe beam. It is then focussed on the sample by a curved mirror. The transmitted/ reflected probe from the sample is then focused and collected by fibre coupled spectrometer. The synchronised optical chopper is used to chop the pump at the frequency of 500 Hz. The induced absorption change ( $\Delta A$ ) is calculated from the difference in absorption of two adjacent probe pulses (with and without pump).

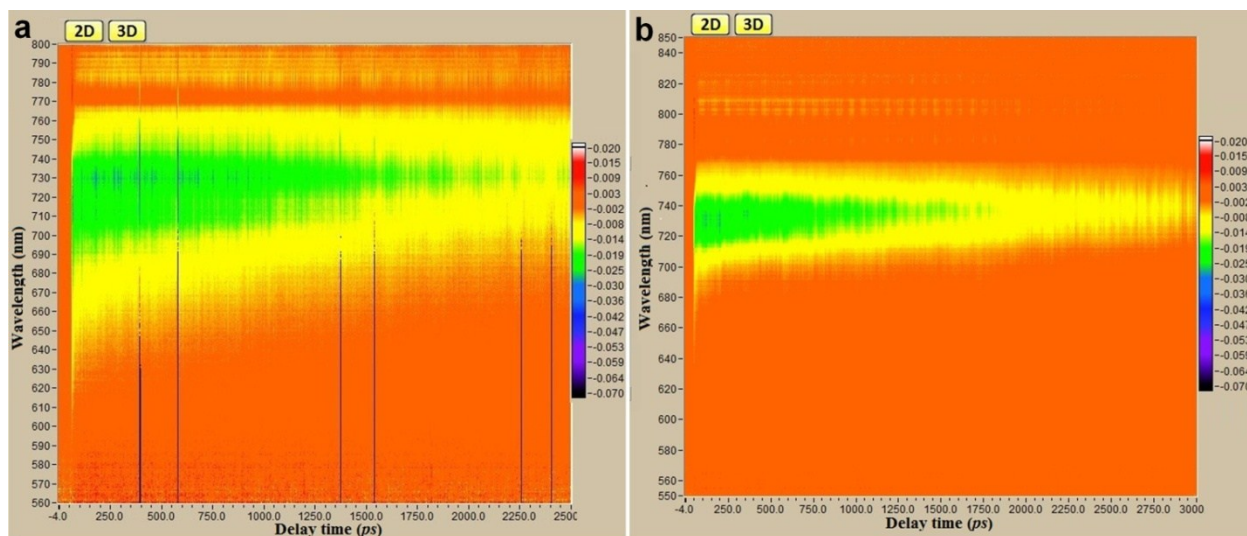


**Fig. S20.** The 3D pseudo-colour map of fs-TAS for (a) unmodified and (b)  $\text{CsPbBr}_{1.5}\text{I}_{1.5}$  QD modified bulk  $\text{CH}_3\text{NH}_3\text{PbI}_{3-x}\text{Cl}_x$ .

**Table S4:** Bleaching wavelength change in TA spectrum for unmodified and different modified bulk perovskite.

| Samples   | Architecture        |                  |                  |
|---|---------------------|------------------|------------------|
|   | w/o ETL/HTL<br>(nm) | With ETL<br>(nm) | With HTL<br>(nm) |
| Unmodified                                      | 728                 | 738              | 724              |
| CB modified                                     | 731                 | 738              | 694              |
| CsPbBr <sub>3</sub> modified                    | 707                 | 703              | 725              |
| CsPbBr <sub>1.5</sub> I <sub>1.5</sub> modified | 716                 | 708              | 718              |
| CsPbBrI <sub>2</sub> modified                   | 719                 | 721              | 707              |

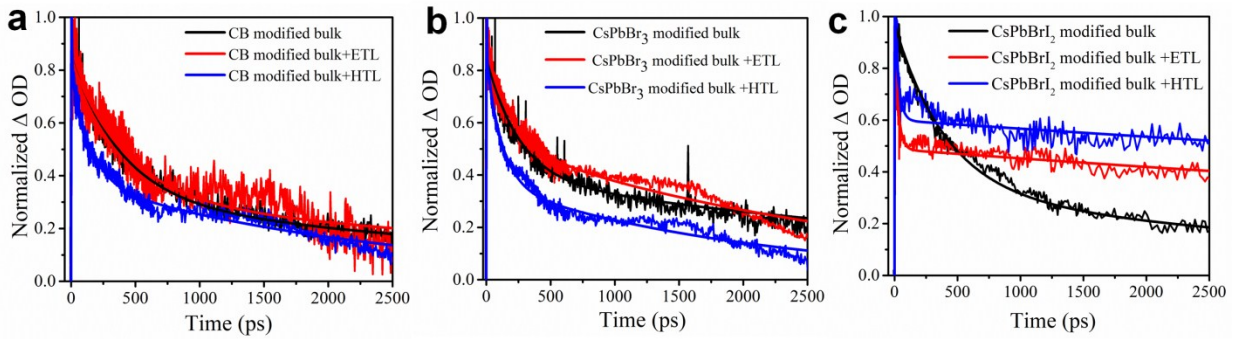


**Fig. S21.** Plots of fs-transient bleach decay kinetics and the corresponding three exponential modified Gaussian fitting for (a) CB, (b) CsPbBr<sub>3</sub> QD and (c) CsPbBrI<sub>2</sub> QD modified bulk CH<sub>3</sub>NH<sub>3</sub>PbI<sub>3-x</sub>Cl<sub>x</sub> film.

**Table S5:** Time components of the CB, CsPbBr<sub>3</sub> QD and CsPbBrI<sub>2</sub> QD modified perovskite films extracted by global fitting of the fs-TAS decay profile.

| Samples                           | $\tau_1$ (ps) | $\tau_2$ (ps) | $\tau_3$ (ps) |
|-----------------------------------|---------------|---------------|---------------|
| CB modified                       | 2.8           | 394           | 4439          |
| CB modified/ETL                   | 4.2           | 409           | 3726          |
| CB modified/HTL                   | 4.7           | 146           | 2436          |
| CsPbBr <sub>3</sub> modified      | 1.2           | 250           | 4922          |
| CsPbBr <sub>3</sub> modified/ETL  | 1.4           | 176           | 2892          |
| CsPbBr <sub>3</sub> modified/HTL  | 2.7           | 120           | 2101          |
| CsPbBrI <sub>2</sub> modified     | 0.9           | 405           | 3898          |
| CsPbBrI <sub>2</sub> modified/ETL | 1.2           | 28            | 13183         |
| CsPbBrI <sub>2</sub> modified/HTL | 1.1           | 30            | 17701         |

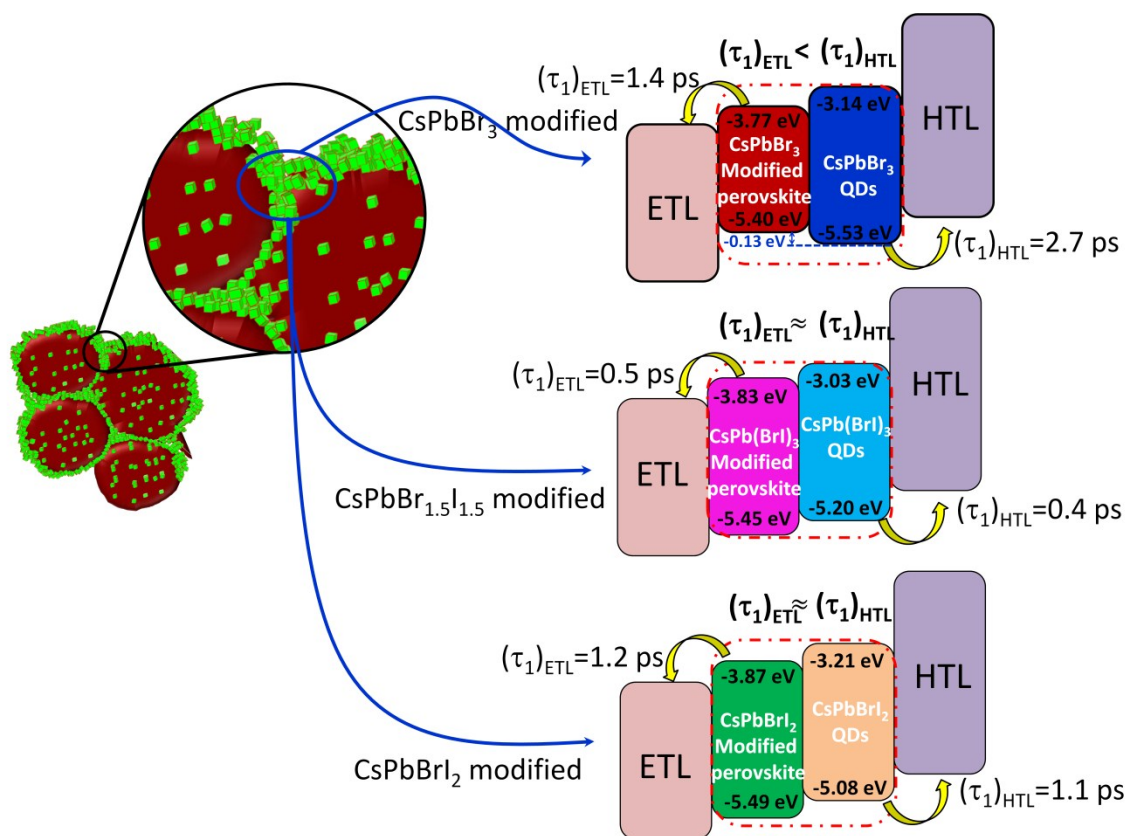


**Fig. S22.** Schematic representation of the energy band positions and electron/hole transfer at the grain boundaries and the associated time constants calculated from fs-TAS measurements.

## References

- S1 H. Yu, F. Wang, F. Xie, W. Li, J. Chen and N. Zhao, *Adv. Funct. Mater.*, 2014, **24**, 7102–7108.
- S2 E. Edri, S. Kirmayer, S. Mukhopadhyay, K. Gartsman, G. Hodes and D. Cahen, *Nat. Commun.*, 2014, **5**, 3461.
- S3 S. D. Stranks, G. E. Eperon, G. Grancini, C. Menelaou, M. J. P. Alcocer, T. Leijtens, L. M. Herz, A. Petrozza and H. J. Snaith, *Science*, 2013, **342**, 341–344.
- S4 L. Wang, C. McCleese, A. Kovalsky, Y. Zhao and C. Burda, *J. Am. Chem. Soc.* 2014, **136**, 12205–12208.
- S5 C. Wehrenfennig, G. E. Eperon, M. B. Johnston, H. J. Snaith and L. M. Herz, *Adv. Mater.*, 2014, **26**, 1584–1589.
- S6 P. Piatkowski, B. Cohen, F. J. Ramos, M. D. Nunzio, M. K. Nazeeruddin, M. Grätzel, S. Ahmad and A. Douhal, *Phys. Chem. Chem. Phys.*, 2015, **17**, 14674–14684.